LIMNOLOGY
and
OCEANOGRAPHY

ASLO

Limnol. Oceanogr. 66, 2021, 4347–4362

doi: 10.1002/lno.11965

Increased petrogenic and biospheric organic carbon burial in sub-Antarctic fjord sediments in response to recent glacier retreat

Sonja Berg,[1*] **Sandra Jivcov**,[1] **Stephanie Kusch**,[2] **Gerhard Kuhn**,[3] **Duanne White**,[4] **Gerhard Bohrmann**,[5] **Martin Melles**,[1] **Janet Rethemeyer**[1]

[1]Institute of Geology and Mineralogy, University of Cologne, Cologne, Germany
[2]CologneAMS—Centre for Accelerator Mass Spectrometry, University of Cologne, Cologne, Germany
[3]Alfred-Wegener-Institut Helmholtz Zentrum für Polar- und Meeresforschung, Bremerhaven, Germany
[4]Centre for Applied Water Science, Institute for Applied Ecology, University of Canberra, Canberra, Australian Capital Territory, Australia
[5]MARUM—Center for Marine Environmental Sciences and Department of Geosciences, University of Bremen, Bremen, Germany

Abstract

Fjords are recognized as hotspots of organic carbon (OC) burial in the coastal ocean. In fjords with glaciated catchments, glacier discharge carries large amounts of suspended matter. This sedimentary load includes OC from bedrock and terrigenous sources (modern vegetation, peat, soil deposits), which is either buried in the fjord or remineralized during export, acting as a potential source of CO_2 to the atmosphere. In sub-Antarctic South Georgia, fjord-terminating glaciers have been retreating during the past decades, likely as a response to changing climate conditions. We determine sources of OC in surface sediments of Cumberland Bay, South Georgia, using lipid biomarkers and the bulk ^{14}C isotopic composition, and quantify OC burial at present and for the time period of documented glacier retreat (between 1958 and 2017). Petrogenic OC is the dominant type of OC in proximity to the present-day calving fronts ($60.4 \pm 1.4\%$ to $73.8 \pm 2.6\%$) and decreases to $14.0 \pm 2.7\%$ outside the fjord, indicating that petrogenic OC is effectively buried in the fjord. Beside of marine OC, terrigenous OC comprises $2.7 \pm 0.5\%$ to $7.9 \pm 5.9\%$ and is mostly derived from modern plants and Holocene peat and soil deposits that are eroded along the flanks of the fjord, rather than released by the retreating fjord glaciers. We estimate that the retreat of tidewater glaciers between 1958 and 2017 led to an increase in petrogenic carbon accumulation of 22% in Cumberland West Bay and 6.5% in Cumberland East Bay, suggesting that successive glacier retreat does not only release petrogenic OC into the fjord, but also increases the capacity of OC burial.

Marine fjords in the high- and mid-latitudes are sites of net sediment accumulation that receive terrigenous input from rivers and erosional products released by glaciers, depending on the characteristics of their catchments (Bianchi et al. 2020). Besides high general sediment accumulation, which is correlated to the magnitude of discharge by rivers and glaciers and associated sediment loads (e.g., Syvitski and Andrews 1994; Overeem et al. 2017), organic carbon (OC) is effectively sequestered in fjord environments (e.g., Kim et al. 2011; Smeaton et al. 2016; Cui et al. 2017). On a global scale, OC deposition in fjord sediments accounts for c. 11% of annual marine carbon burial, making them hotspots of global carbon burial (Smith et al. 2015). The composition of organic matter (OM) in fjord sediments depends on the predominant OC sources, which can be classified as (i) autochthonous aquatic biomass (OC_{marine}), (ii) terrigenous OC (OC_{terr}) derived from terrestrial vegetation as well as soils and peat deposits in the catchment, and (iii) petrogenic carbon (OC_{petro}), OC of biological origin that has been preserved in sedimentary or metamorphic rocks over geological time scales. OC_{marine} and OC_{terr} represent the biospheric pool within the active carbon cycle, whereas OC_{petro} is part of the geological carbon cycle.

While modern biospheric OC is neutral with respect to the atmospheric carbon budget (fixation vs. respiration; input = output) and burial of this material may remove OC from the active carbon cycle, OC_{petro} export is a potential source of CO_2 to the atmosphere when this previously sequestered OC pool is remineralized rather than reburied (Galy et al. 2007,

*Correspondence: sonja.berg@uni-koeln.de

Additional Supporting Information may be found in the online version of this article.

2015). OC_{petro} is the dominant component, when glaciers or rivers discharge large amounts of eroded bedrock, particularly if the eroded lithologies are rich in OC (e.g., Kim et al. 2011; Cui et al. 2016*a*; Vonk et al. 2019). Despite its refractory nature, partial oxidation of OC_{petro} occurs during riverine transport and on shelves (Galy et al. 2007) and has been suggested to contribute to atmospheric CO_2 over glacial–interglacial time scales (Galy et al. 2015). In contrast, rapid reburial, for example, in fjords, may be a process that largely prevents remineralization of this material/old carbon, hence having no effect on active carbon cycling (Smith et al. 2015).

In temperate regions, where glaciers are absent and input of OC_{petro} is low, modern OC_{terr} is a major OC component of fjord sediments (e.g., Cui et al. 2017). High contribution of OC_{terr} in near-shore marine sediments is also found in the Arctic (e.g., Winkelmann and Knies 2005). Here, OC_{terr} exported to the coastal oceans contains considerable proportions of OC_{terr} that was previously locked in permafrost soils and is released by (thermal) erosion (e.g., Vonk et al. 2019; Kusch et al. 2021*a*). In contrast to modern OC_{terr}, (permafrost) soil OC represents a carbon pool that can act as an atmospheric carbon source, when remineralized.

In order to better understand processes that affect burial of OC in response to climatic changes in coastal areas, and fjords in particular, sources to sedimentary OC need to be distinguished and quantified.

Approaches to distinguish OC sources in fjord sediments are mostly based on isotopic (e.g., $\delta^{13}C$, $\delta^{15}N$, $\Delta^{14}C$), elemental (e.g., C/N ratio) and/or lipid biomarker (e.g., *n*-alkanes, fatty acids, lignin phenols, glycerol dialkyl glycerol tetraethers [GDGTs]) proxies (e.g., Winkelmann and Knies 2005; Kim et al. 2011; Cui et al. 2016*a*). In addition to comparative multiproxy analysis, combining lipid biomarker abundances with carbon isotope data can aid at resolving underconstrained isotope mass balance calculations (e.g., Kim et al. 2011). For this purpose, both fatty acids and GDGTs may be among the most versatile lipid compound classes, allowing independent yet internally (compound-class) normalized identification of aquatic and terrigenous contributions to the sediment. High-molecular-weight *n*-fatty acids (even chain lengths $C_{26:0}$, $C_{28:0}$, and $C_{30:0}$) derive from leaf waxes of higher land plants (Eglinton and Hamilton 1967; Diefendorf and Freimuth 2017) and branched GDGTs (brGDGTs) primarily are membrane lipids of soil-living bacteria and have been applied as a proxy for the input of soil OM in marine sediments (e.g., Hopmans et al. 2004). In contrast, low-molecular-weight fatty acids (including $C_{14:0}$, $C_{16:0}$, and $C_{18:0}$) are the dominant fatty acids in phytoplankton, and crenarchaeol, an isoprenoid GDGT, is predominantly produced by marine Thaumarchaeota (e.g., Volkman et al. 1998; Schouten et al. 2013). Accordingly, high molecular weight vs. low molecular weight and brGDGT vs. crenarchaeol abundances can provide quantitative information about the relative contribution from terrigenous and marine OC to sediments, thus, providing constraints about the relative abundances of different OC pools for multi-endmember mass balances.

In this study, we focus on a fjord system in the sub-Antarctic (South Georgia), a region that is sensitive to climate variability and has experienced periods of considerable glacier mass changes during the Holocene (e.g., Bentley et al. 2007; White et al. 2018). In recent decades, rates of glacier retreat have been increasing on South Georgia, leading to progressive retreat of tidewater glaciers, particularly on the northeastern side of the island (Fig. 1; Gordon et al. 2008; Cook et al. 2010; Farias-Barahona et al. 2020). To investigate how OC burial has changed in relationship to the observed glacier retreat between 1958 and 2017, we characterize the composition of OC sources in Cumberland Bay, one of the largest fjord systems in South Georgia (Fig. 1). In particular, we focus on the quantification of OC_{terr} and OC_{petro} in surface sediments to investigate allochthonous OC input and burial in the fjords based on the fjord geometries before and after recent glacier retreat. We use a combination of lipid biomarker ratios and $\Delta^{14}C$ endmembers to constrain mixing models that allow for the quantification of marine, terrigenous and petrogenic OC in the fjord sediments. Based on this data set, we provide first estimates of OC_{terr} and OC_{petro} mass accumulation rates (MARs) in a sub-Antarctic fjord and show how absolute OC_{terr} and OC_{petro} accumulation has changed in response to documented recent (1958–2017) glacier retreat.

Study site

Today, ice caps, snow fields and glaciers are covering c. 63% of the island of South Georgia (54°S, 36°W), which is located c. 350 km to the south of the Polar Front but to the north of the present-day winter sea-ice limit (Orsi et al. 1995). On South Georgia, the climatic conditions and topography result in a glaciologically highly dynamic setting. Smaller cirque glaciers as well as larger land-terminating and sea-calving glaciers respond to changing climatic conditions by changes in mass balance, extent, and erosion rates (e.g., van der Bilt et al. 2017).

Especially the northern coast of the island is characterized by fjords, which are connected to glacially eroded troughs on the shelf that mark former pathways of large outlet glaciers and ice streams (Hodgson et al. 2014; Graham et al. 2017). Cumberland Bay consists of two c. 15 km long fjords (Cumberland East Bay and Cumberland West Bay). Bathymetric surveys found a maximum water depth of c. 270 m in both fjords and submarine moraine ridges that reflect past changes in glacier extent (Hodgson et al. 2014). In Cumberland East Bay, three sea-calving glaciers drain into the fjord, the Hamberg, Harker, and Nordenskjöld Glaciers, the latter being the largest glacier on the island (Gordon et al. 2008). In Cumberland West Bay, Neumayer, Geikie, and Lyell Glaciers drain into the fjord. Neumayer Glacier shows the highest thinning rates and area loss of the glacier on the island (Farias-Barahona et al. 2020). Little Jason Lagoon, a marine inlet on the

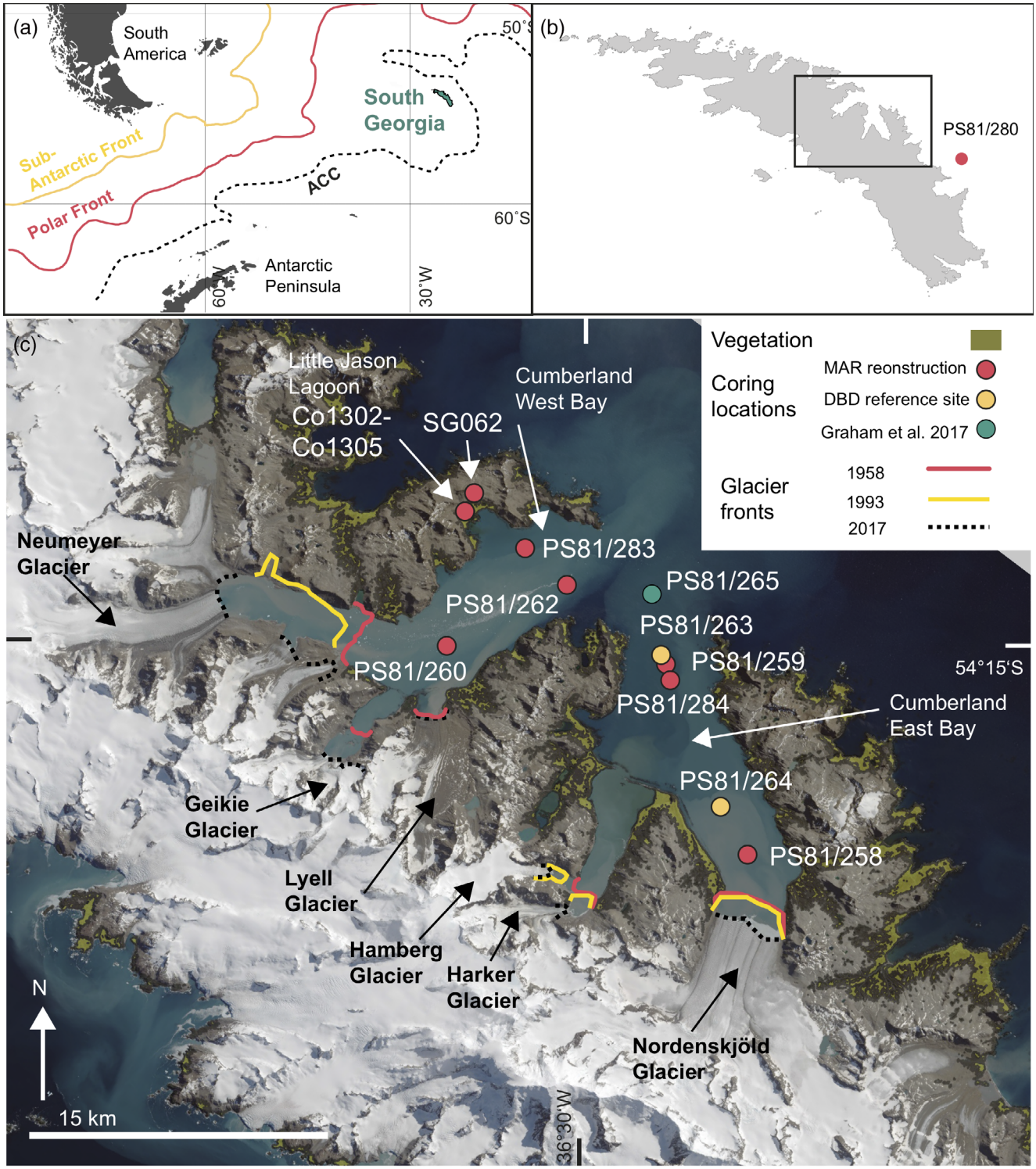

Fig 1. (**a**) Position of the island of South Georgia in the Atlantic sector of the Southern Ocean (southern boundary of the Antarctic Circumpolar Current, ACC; fronts after Orsi et al. 1995); (**b**) locations of Cumberland West Bay and East Bay on the northeastern side of the island and coring site PS81/280 on the shelf; (**c**) Landsat8 image of Cumberland bays showing the input of detrital matter from the adjacent glaciers. Coring locations and names of glaciers mentioned in the text are indicated (DBD, dry bulk density). Highlighted in green are low-lying coastal areas covered by vegetation (satellite image accessed from Quantarctica 3; position of glacier fronts and vegetation coverage accessed from https://sggis.gov.gs).

northwestern shore of Cumberland West Bay, is connected to the fjord by a shallow subaquatic sill (~ 1 m) and has a maximum water depth of 24 m in the center (Fig. 1, Berg et al. 2019).

Bedrock in the catchment of Cumberland Bay consists of Mesozoic greywacke and pelites that contain volcanoclastic components but also marine sediments, which could be a source of petrogenic OC (Cumberland Bay and Sandebugten formations; McDonald 1982). Areas below 200 m altitude are covered by vegetation (Fig. 1), consisting of tussock grass along the coastal lowlands, whereas bryophyte assemblages and lichen dominate at higher altitude. In the cool and moist maritime climate, soils and peat deposits form at lower altitude.

Materials and methods

Transects along land to fjord to open ocean and from glacier proximal to glacier distal sites were sampled during *RV* Polarstern cruise PS81 (Bohrmann 2013). Sediment cores were retrieved from nine stations in Cumberland West Bay and Cumberland East Bay (Table 1). Sediment samples from seven stations provided undisturbed core tops and were used to study spatial changes in OC content and composition in the fjord sediments. One surface sample from the shelf (station PS81/280-2) was taken as well as a representative endmember for fully marine conditions (Fig. 1; Table 1). In addition to the fjord sediments, four sites in the adjacent Little Jason Lagoon were sampled, which was used as a reference site not affected by direct glacier input. Samples were retrieved using multicorer and gravity core devices in Cumberland Bay and gravity or piston corer (UWITEC, Austria) in Little Jason Lagoon (Table 1). The samples comprise the uppermost 0–2 or 0–4 cm of opened sediment cores. For core PS81/284-1, 5–6 cm was sampled, since the upper 5 cm was lost during coring. On a late Pleistocene moraine ridge in the catchment of Cumberland West Bay, a peat profile (Profile SG062) was excavated and sampled at an altitude of c. 32 m above sea level to characterize the $\Delta^{14}C$ value of the terrigenous endmember (Fig. 1, *see* Supporting Information). Soil characteristics and thicknesses were investigated across a range of representative landforms around Enten and Jason Valleys (Supporting Information Fig. S1). Soil thickness profiles were mapped at approximately 30 sites either in shallow soil pits or in natural sections. Soil sections across raised beaches and dune systems in these valleys were also systematically surveyed using a sediment probe and stream sections.

Sediments were freeze-dried and ground for further analyses. Total organic carbon (TOC) content was measured with a DIMATOC 100 carbon analyzer (Dimatec Corp.) and total nitrogen (N) content was measured with a Vario Micro Cube combustion elemental analyzer (Elementar).

Lipids were extracted by accelerated solvent extraction (ASE300, Thermo Scientific) with dichloromethane (DCM) : methanol (9 : 1, v : v) at 120°C and 75 bar. The total lipid

Table 1. Samples analyzed and discussed in this study, with coordinates of coring locations, water depth/altitude and device used for coring (*see* also Bohrmann 2013).

Core	Latitude	Longitude	Altitude relative to sea level (m)	Coring device
Little Jason Lagoon				
Co1302	54.191667°S	36.594300°W	−15.7	GC
Co1303	54.192467°S	36.594967°W	−15.8	GC
Co1304	54.192583°S	36.588683°W	−15.7	GC
Co1305	54.192800°S	36.591150°W	−15.8	PC
SG062	54.189286°S	36.589241°W	+32	Pit
Cumberland East Bay				
PS81/258-3	54.337000°S	36.388833°W	−178	MUC
PS81/259-1	54.261333°S	36.437667°W	−262	MUC
PS81/263-1	54°261,000°S	36.439167°W	−263	GC
PS81/284-1	54.265200°S	36.437167°W	−259	GC
PS81/264-1	54.322833°S	36.400833°W	−176	GC
PS81/265-1	54.236000°S	36.443166°W	−211	GC
Cumberland West Bay				
PS81/260-1	54.246667°S	36.582167°W	−216	MUC
PS81/262-1	54.224833°S	36.511833°W	−234	MUC
PS81/283-1	54.215333°S	36.538000°W	−193	GC
Shelf				
PS81/280-2	54.457333°S	35.842500°W	−237	MUC

GC, gravity corer; MUC, multicorer; PC, piston corer.

extract (TLE) was desulfurized using activated copper and was saponified with 0.5 M KOH in methanol : water (9 : 1, v : v) at 80°C for 2 h. Neutral lipids were isolated from the TLE by liquid–liquid extraction with DCM after addition of water and were then separated into polarity fractions using silica gel open column chromatography (SiO_2, deactivated with 1% H_2O, 60 Å), GDGTs were recovered in methanol. For GDGT analysis, a C_{46} GDGT standard was added and the samples were filtered over PTFE filters (0.45 μm × 4 mm) using hexane : isopropanol (95 : 5, v : v). GDGTs were analyzed on an Agilent 1290 UHPLC connected to an Agilent 6460 QQQ equipped with an APCI ion source following the method of Hopmans et al. (2016). GDGTs were analyzed in SIM mode and quantified according to Huguet et al. (2006).

Fatty acids were recovered from the remaining TLE–water mixture using DCM after acidification to pH 1. Subsequently, the acidic fraction was transesterified under an N_2 atmosphere at 80°C overnight using MeOH : HCl (95 : 5, v : v). The resulting fatty acid methyl esters (FAMEs) were isolated by hexane extraction and further separated into two polarity fractions by silica gel open column chromatography (4 cm × 0.5 cm, deactivated, 60 Å), topped off with Na_2SO_4 to remove any residual water. FAMEs were recovered in hexane. FAMEs were identified and quantified with an Agilent 7890B GC-FID against an authentic external standard mixture as described in Berg et al. (2019).

For radiocarbon analysis, aliquots of the sediment samples (1 g) were decarbonized with dilute HCl (0.5%). Acid-insoluble OC was converted into graphite and Accelerator Mass Spectrometry (AMS) ^{14}C measurements were carried out at the CologneAMS facility (Rethemeyer et al. 2019). All ^{14}C results are reported as $\Delta^{14}C$ (‰) and conventional ^{14}C ages (^{14}C yr BP) following the conventions by Stuiver and Polach (1977).

Results

$\Delta^{14}C$ values in fjord sediments range from -360 ± 3‰ to -729 ± 3‰ (corresponding to 3525 ± 35 to $10{,}420 \pm 70$ ^{14}C yr BP). The most depleted values occur at sites PS81/260 (-711 ± 2‰, corresponding to 9910 ± 65 ^{14}C yr BP) and PS81/283 (-729 ± 3‰, corresponding to $10{,}420 \pm 70$ ^{14}C yr BP), which are closest to the calving front of Neumayer Glacier (Fig. 2a). Offshore site PS81/280, which is farthest from glacier input, provided the least depleted $\Delta^{14}C$ value of -228 ± 4‰ (corresponding to 2020 ± 40 ^{14}C yr BP; Fig. 2a). All these ^{14}C ages exceed the local marine reservoir age of c. 1100 yr ($\Delta^{14}C = -133$‰; Graham et al. 2017). Although samples integrate 1–4 cm of sediment (Table 2), sedimentation rates of 1–2 m ka^{-1} in Cumberland Bay (Graham et al. 2017; Berg et al. 2020) imply that the samples only integrate a time span of 5–40 yr, thus, the depositional age falls within the analytical uncertainty of the ^{14}C analysis.

In Little Jason Lagoon, $\Delta^{14}C$ values at the four investigated sites agree within 1σ analytical error from -138 ± 4‰ to -145 ± 4‰ (corresponding to 1130 ± 35 to 1190 ± 35 ^{14}C yr BP) (Fig. 2a; Table 2) and mirror the marine reservoir age off South Georgia reported by Graham et al. (2017).

TOC contents in the surface sediments of Cumberland Bay and on the shelf range from 0.4 to 0.8 wt% and are around 3 wt% in Little Jason Lagoon (Fig. 2; Table 2). All samples contain plant wax-derived high-molecular-weight fatty acids (here $C_{26:0}$, $C_{28:0}$, and $C_{30:0}$ fatty acids), soil-derived brGDGTs as well as biomarkers of mostly marine origin: low-molecular-weight fatty acids (here $C_{14:0}$, $C_{16:0}$, and $C_{18:0}$ fatty acids) and crenarchaeol (Fig. 3; Supporting Information Table S1). The proportions of the terrigenous to marine OM to the biospheric OM pool were constrained using biomarker ratios. Based on fatty acid concentrations, we calculated fractional abundances of terrigenous OM (FA_{terr}) using $FA_{terr} = (C_{26:0} + C_{28:0} + C_{30:0})/([C_{14:0} + C_{16:0} + C_{18:0}] + [C_{26:0} + C_{28:0} + C_{30:0}])$ and based on GDGTs using $GDGT_{terr} =$ brGDGTs/(brGDGTs + crenarchaeol). (brGDGT = IIIa + IIIa′ + IIa + IIa′ + Ia; analogous to the calculation of the branched vs. isoprenoid tetraether (BIT) index; Hopmans et al. 2004). Fatty acids indicate FA_{terr} ranging from 0.08 to 0.22, with highest values at site Co1304 in Little Jason Lagoon ($FA_{terr} = 0.16$) and at site PS81/258 in Cumberland Bay ($FA_{terr} = 0.22$), just off the calving front of Nordenskjöld Glacier (Fig. 2).

For the fjord sites, the GDGT-based ratios indicate terrigenous contributions of $GDGT_{terr} = 0.033$–0.067 (with exception of site PS81/283 with $GDGT_{terr} = 0.516$), which is comparable to the fatty acid-derived estimates at all stations in the fjord. In Little Jason Lagoon, however, GDGTs with $GDGT_{terr} = 0.852$–0.970 provide much higher abundances of terrigenous OM than fatty acids (Fig. 2).

Discussion

Biomarker sources

Estimates of the relative contributions of terrestrial and marine OC in the investigated sediments using fatty acids and GDGTs agree well for the Cumberland Bay fjord sediments (offsets between FA_{terr} and $GDGT_{terr}$ ranging from 0.03 to 0.18), but are substantially different for the core-tops in Little Jason Lagoon ($GDGT_{terr}$ is 0.75–0.85 higher than FA_{terr}) (Fig. 2; Table 2). The FA_{terr} estimates in Little Jason Lagoon may be biased by differential preservation of individual compounds within one compound class but could also be caused by different origin (soil vs. terrestrial plants) and alternative source organisms producing the respective terrigenous/marine biomarkers. We expect minor preservation biases, due to high sedimentation rates, shallow water depth and short transport distances, and rather consider the source/origin of fatty acids and GDGTs to primarily explain our observations. Whereas the majority of high-molecular-weight fatty acids ($C_{26:0}$ to

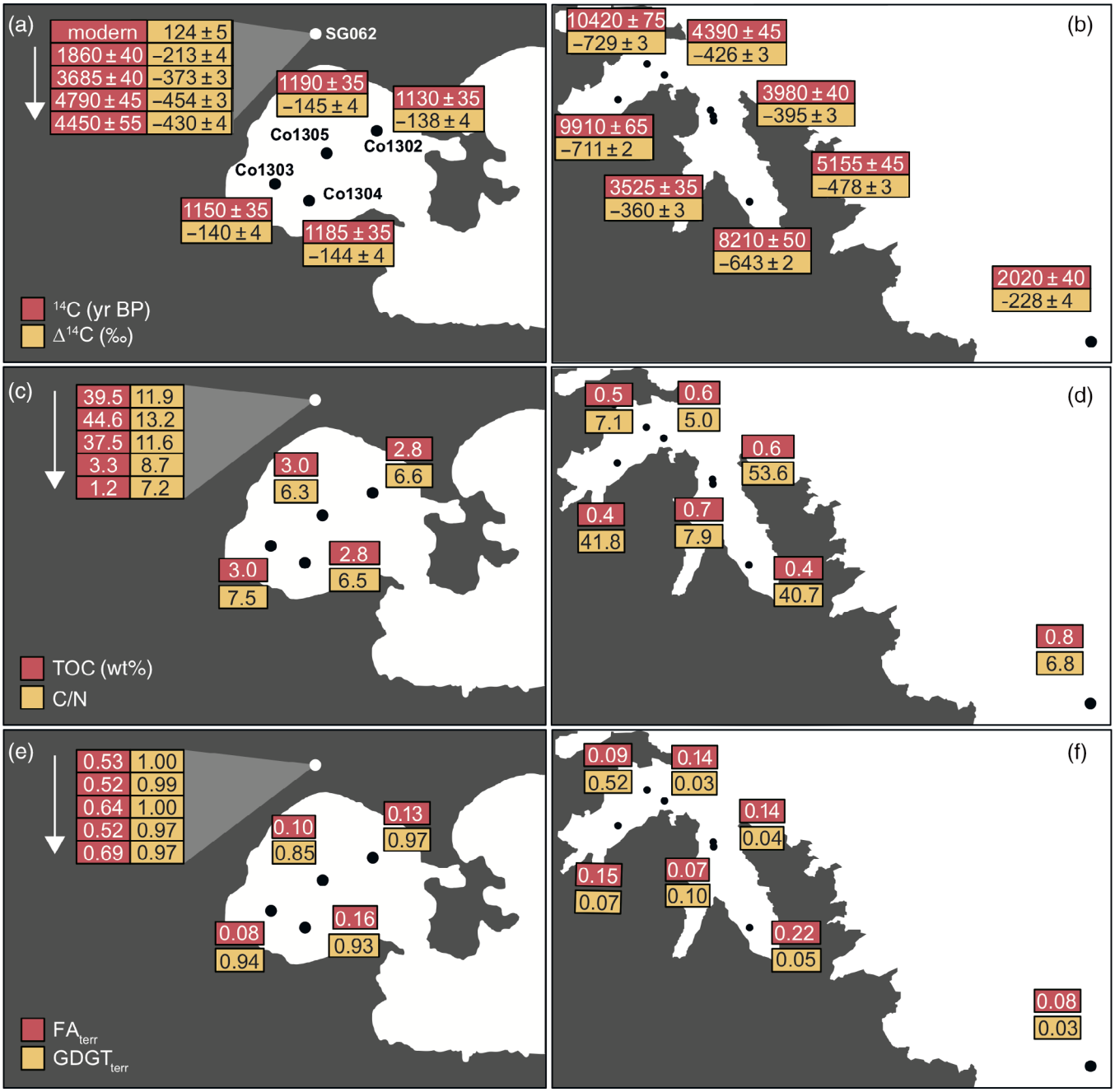

Fig 2. Conventional ^{14}C ages (yr BP) and $\Delta^{14}C$ isotope values (‰) of bulk OC (**a**,**b**), TOC content and TOC/N ratios (**c**,**d**) and fractional abundances of terrigenous OM derived from fatty acid (FA) and GDGTs ratios in the peat profile (site SG062) and surface sediments (**e**,**f**) of Little Jason Lagoon (maps left: **a**, **c**, **e**), Cumberland bays and from the shelf site PS81/280 (maps right; **b**, **d**, **f**). More information on the stratigraphy of SG062 is given in Table 2 and in the Supporting Information).

$C_{32:0}$) can be assigned to a leaf wax origin, alternative sources such as microalgae (Volkman et al. 1980; Schouten et al. 1998) and microbes (Li et al. 2018; Chen et al. 2019) have previously been reported, which would lead to an overestimation of FA_{terr} in the marine sediments. Alternatively, contribution of low-molecular-weight fatty acids from terrestrial sources including bacteria and plants may result in an overestimation of the marine contribution based on the fatty acid ratio. Low-molecular-weight fatty acid concentrations in the fjords are higher (roughly one order of magnitude) than corresponding high-molecular-weight fatty acid concentrations, and typically higher than in the peat deposits from the catchment of Cumberland Bay (Fig. 3a–d), supporting a primarily aquatic origin. However, the abundance of low- and

Table 2. Bulk sediment and biomarker data from South Georgia fjord sediments: ^{14}C data and TOC contents, fractional abundances of terrigenous organic matter derived from high-molecular-weight/low-molecular-weight fatty acids (FA) and brGDGTs/crenarchaeol (GDGT). $\#rings_{tetra}$ index > 0.7 indicates in situ production of brGDGTs in marine sediments (Sinninghe Damsté 2016).

Core	Depth (cm)	AMS ID	$\Delta^{14}C$ (‰)	$F^{14}C$	^{14}C age	TOC (wt%)	FA_{terr}	$GDGT_{terr}$	$\#rings_{tetra}$
Co1302	0–2	COL2891	−138 ± 4	0.8690 ± 0.0040	1130 ± 35	2.8	0.13	0.97	0.11
Co1303	0–2	COL2892	−140 ± 4	0.8670 ± 0.0040	1150 ± 35	3.0	0.08	0.94	0.12
Co1304	0–2	COL2893	−144 ± 4	0.8630 ± 0.0040	1185 ± 35	2.8	0.16	0.93	0.13
Co1305	0–2	COL2894	−145 ± 4	0.8620 ± 0.0040	1190 ± 35	3.0	0.10	0.85	0.16
PS81/258–3	0–2	COL3657	−643 ± 2	0.3598 ± 0.0023	8210 ± 50	0.4	0.22	0.05	0.59
PS81/259–1	0–2	COL3658	−478 ± 3	0.5265 ± 0.0030	5155 ± 45	0.6	0.14	0.04	0.65
PS81/263–1	2–4	COL2585	−395 ± 3	0.6095 ± 0.0032	3980 ± 40	—	—	—	—
PS81/284–1	5–6	COL2903	−360 ± 3	0.6448 ± 0.0029	3525 ± 35	0.7	0.10	0.05	0.71
PS81/260–1	0–2	COL3659	−711 ± 2	0.2912 ± 0.0024	9910 ± 65	0.4	0.15	0.07	0.40
PS81/262–1	0–2	COL3660	−426 ± 3	0.5792 ± 0.0031	4390 ± 45	0.6	0.14	0.03	0.62
PS81/283–1	1–2	COL4988	−729 ± 3	0.2733 ± 0.0024	10,420 ± 70	0.5	0.09	0.52	0.53
PS81/280–2	0–2	COL3661	−228 ± 4	0.7777 ± 0.0038	2020 ± 40	0.8	0.08	0.03	0.82
SG062	0–18	COL5333	124 ± 5	1.1327 ± 0.0051	> Modern	39.5	0.53	0.99	0.02
SG062	30–45.5	COL5335	−213 ± 4	0.7936 ± 0.0038	1860 ± 40	44.6	0.52	0.99	0.02
SG062	60–70	COL5336	−373 ± 3	0.6322 ± 0.0033	3680 ± 40	37.5	0.63	0.99	0.01
SG062	110–135	COL5338	−454 ± 3	0.5506 ± 0.0032	4790 ± 45	3.3	0.52	0.97	0.01
SG062	135–155	COL5340	−430 ± 4	0.5748 ± 0.0039	4450 ± 55	1.2	0.69	0.97	0.02
SG062*	0–18	COL5334	−131 ± 4	0.8761 ± 0.0044	1060 ± 40	—	—	—	—

*Seal hair from peat surface of profile SG062, reflecting recent marine reservoir age.

high-molecular-weight fatty acids is relatively similar in the peat deposits, which have a mean FA_{terr} of 0.56 ± 0.06 ($n = 3$), indicating that plant/peat-derived fatty acids may contribute to the low-molecular-weight fatty acid pool in the marine sediments (Fig. 3). Yet, a predominantly aquatic origin of low-molecular-weight fatty acids in the marine sediments of Cumberland Bay and Little Jason Lagoon is supported by their compound-specific ^{14}C ages in comparison to those of the concurrent high-molecular-weight fatty acids (Berg et al. 2020). However, we cannot exclude low-molecular-weight fatty acid contributions from plants/peat a priori.

Branched GDGT concentrations in the fjords are roughly an order of magnitude lower than concurrent crenarchaeol concentrations (similar to high-molecular-weight vs. low-molecular-weight fatty acids; Fig. 3; Supporting Information Table S1), as could be expected if brGDGTs are primarily sourced from land and crenarchaeol produced in the water column. However, brGDGT *in situ* production by sedimentary bacteria can mimic a terrestrial signal, which could explain higher GDGT-based terrestrial OM estimates in Little Jason Lagoon, but can be assessed using the #ringstetra index (Sinninghe Damsté 2016). For Little Jason Lagoon, low #ringstetra values support a high terrigenous input and negligible in situ production of brGDGTs (Table 2; Sinninghe Damsté 2016). In contrast, #ringstetra is relatively high throughout Cumberland Bay, although the index is only above 0.7 (indicating *in situ* production of brGDGTs) only at fjord sites PS81/283, PS81/284, and the shelf site PS81/280. Thus, overestimation (if any) of the terrigenous fraction is only likely for the fjord sediments (not for Little Jason Lagoon), however, we note that GDGT-derived estimates are still much lower than the FA-derived fractional abundances in these samples (Fig. 2e,f). Crenarchaeol is also produced by soil Thaumarchaeota (Sinninghe Damsté et al. 2012; Kusch et al. 2019) and present in the peat deposits at concentrations similar to those observed in the Little Jason Lagoon sediments (Fig. 3g), thus, we cannot exclude that the crenarchaeol in Little Jason Lagoon is in fact also supplied from the catchment rather than produced in the marine inlet. However, low archaeal productivity (as evident from the very low crenarchaeol concentrations in Little Jason Lagoon compared to the fjord, where they are up to three orders of magnitude higher) due to unfavorable habitat conditions, in particular the shallow water depth in the inlet (Schouten et al. 2013), is a more likely scenario and may in fact result in overestimation of the terrigenous contribution. Nonetheless, we cannot conclusively determine whether aquatic crenarchaeol production is too low or whether crenarchaeol in part has a terrestrial origin in Little Jason Lagoon.

Our biomarker data provide relatively consistent estimates of OM_{terr} for the fjord sediments, but we cannot unequivocally determine which process is responsible for the observed differences in OM_{terr} obtained using either fatty acids or GDGTs in Little Jason Lagoon. We thus use both estimates as well as their mean to calculate the biospheric and petrogenic OC contributions in our samples.

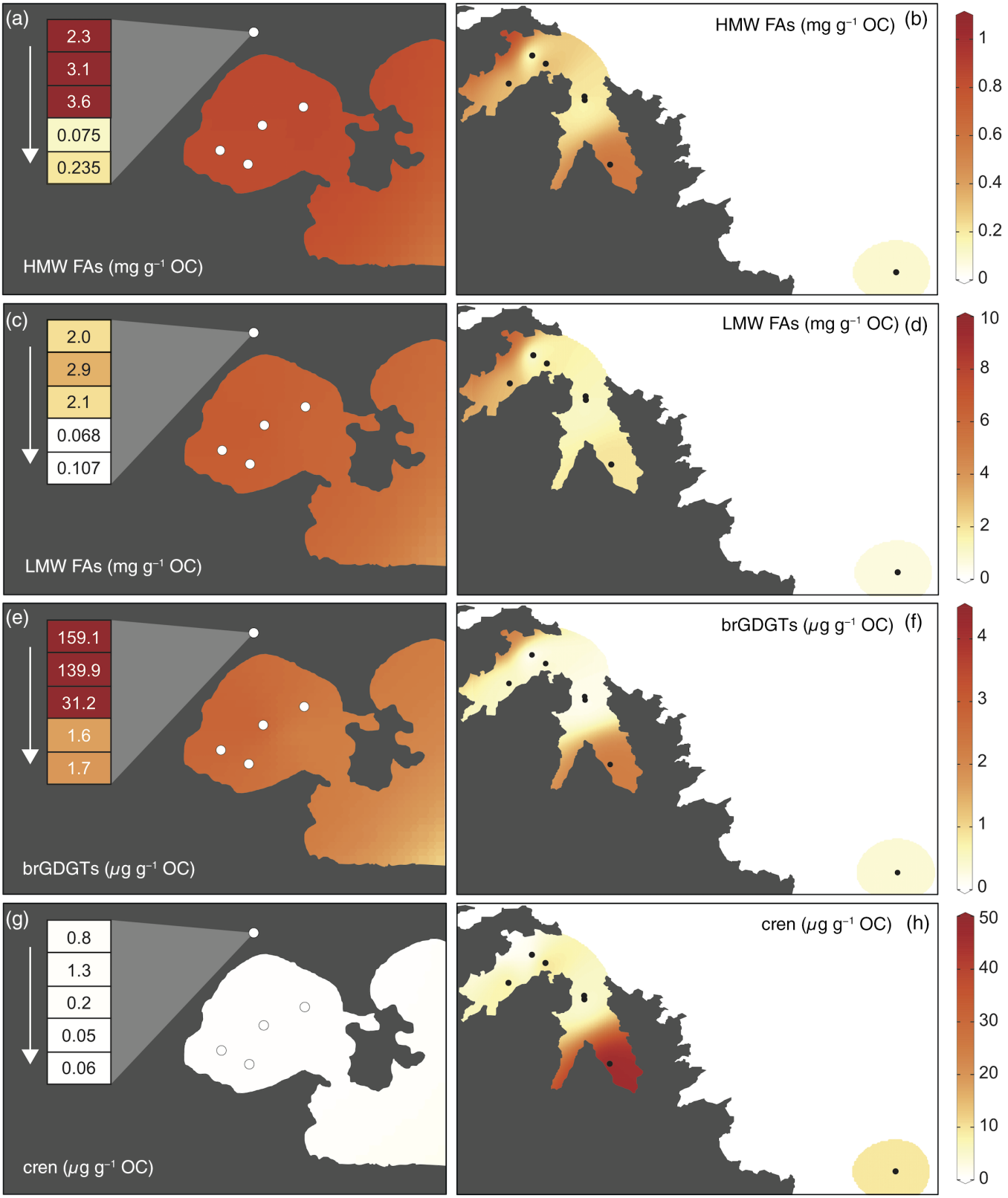

Fig 3. Concentrations of high-molecular-weight (HMW) ($C_{26:0} + C_{28:0} + C_{30:0}$) fatty acids (FA), low-molecular-weight (LMW) ($C_{14:0} + C_{16:0} + C_{18:0}$) FA, and brGDGTs (IIIa + IIIa′ + IIa + IIa′ + Ia), and crenarchaeol in the peat profile SG062, and in surface sediments of Little Jason Lagoon (maps left: **a**, **c**, **e**, **g**), Cumberland bays and from the shelf site PS81/280 (maps right; **b**, **d**, **f**, **h**). More information on the stratigraphy of SG062 is given in Table 2 and in the Supporting Information.

OM contributions

OC contents in the sediments of Cumberland Bay are low, which illustrates that sedimentation in Cumberland Bay is strongly dominated by siliciclastic input, most likely driven by glacier discharge into the fjord (Fig. 2(c)-(d)). In order to distinguish the different OC sources in the sediments, we quantify the contributions of marine and terrigenous OC (biospheric OC), and petrogenic OC with simple iterative mixing models, based on specific $\Delta^{14}C$ endmembers for each source and the relative contributions of terrestrial and marine OC as defined using biomarkers.

First, we use a two end member-mixing model to constrain the biospheric $\Delta^{14}C$ endmember:

$$\Delta^{14}C_{biospheric} = FA_{marine} \times \Delta^{14}C_{marine} + FA_{terr} \times \Delta^{14}C_{terr}, \quad (1)$$

where

$$FA_{marine} = 1 - FA_{terr}. \quad (2)$$

Second, we use the biospheric $\Delta^{14}C$ endmember to determine the relative contribution of petrogenic OC (or another ^{14}C-free OC source) using:

$$f_{petro} = \left(\Delta^{14}C_{bulk} - \Delta^{14}C_{biospheric}\right) / \left(\Delta^{14}C_{petro} - \Delta^{14}C_{biospheric}\right), \quad (3)$$

where $\Delta^{14}C_{marine}$, $\Delta^{14}C_{terr}$, and $\Delta^{14}C_{petro}$ are the respective $\Delta^{14}C$ endmembers of marine, terrigenous, and petrogenic OC. FA_{marine} and FA_{terr} are the fractional abundances of marine and terrigenous OC as defined using FA_{terr} and $GDGT_{terr}$, and f_{petro} is the fractional abundance of the petrogenic endmember. We report the mean ($\pm 1\sigma$) contributions of terrigenous, marine, and petrogenic OC for each site, resulting from models spanning the range of $\Delta^{14}C$ values defined for the two biogenic endmembers.

$\Delta^{14}C_{petro}$ is defined as −1000‰. For the marine endmember ($\Delta^{14}C_{marine}$), we assume a $\Delta^{14}C$ range from −85‰ to −133‰ (corresponding to a reservoir age of 645–1100 yr). A higher value of −85‰ is derived from $C_{16:0}$ fatty acid $\Delta^{14}C$ isotopic composition obtained from surface sediments at site PS81/283 in Cumberland West Bay, which likely reflects the marine reservoir age in the inner fjord (Berg et al. 2020). A lower $\Delta^{14}C$ value is derived from benthic foraminifers from surface sediments in the fjord and on the shelf of South Georgia (Graham et al. 2017; Berg et al. 2020). A similar $\Delta^{14}C$ value of -131 ± 4‰ is obtained for seal hair, sampled on top of a modern peat deposit on the north-western shore of Cumberland West Bay, which is frequently visited by fur and elephant seals (Table 2; *see* Supporting Information). This value (−133‰) likely reflects the reservoir age of circumpolar deep water, which forms the bottom water on the South Georgia shelf and Cumberland Bay (Geprägs et al. 2016). For the mixing models we, thus, use a $\Delta^{14}C_{marine}$ of -109 ± 24‰.

Defining the $\Delta^{14}C$ isotopic composition of the terrigenous endmember ($\Delta^{14}C_{terr}$) contains a larger uncertainty, since terrestrial input is heterogeneous with respect to its $\Delta^{14}C$ signature (Kusch et al. 2021*b*). The terrigenous OM consists of fresh plants with a modern $\Delta^{14}C$ isotopic composition but may also contain contributions from peat deposits and soils, which provide a similar biomarker signature but more depleted $\Delta^{14}C$ values. Formation of peat deposits and soils in the low altitude areas of South Georgia started around the onset of the Holocene (e.g., Van der Putten and Verbruggen 2005). However, the majority of peat and soil, which is presently eroded and deposited in the fjord, likely formed after an expansion of cirque glaciers during the mid-Holocene (Berg et al. 2019). Radiocarbon analysis of a peat profile and underlying sediments, which we sampled on the northwestern shore of Cumberland West Bay support previous studies and indicate the onset of peat formation in the catchment of Little Jason Lagoon between 5500 and 3960 cal yr BP (*see* Supporting Information for description and details on sampling and analyses). The $\Delta^{14}C$ value of 121‰ for plant remains in the upper 0–18 cm indicate the presence of bomb-^{14}C, thus, decadal biomass, and we use this value as the upper limit for the terrestrial endmember. We define the lower limit using the mean $\Delta^{14}C$ value (−154‰) of the upper, OC-rich part of the investigated peat profile (Fig. 2). A more depleted $\Delta^{14}C$ value, thus, absence of bomb-^{14}C, for the lower limit of the terrigenous endmember is supported by a $\Delta^{14}C$ value of −116‰ determined for $C_{26:0}$ fatty acid from a surface sediment sample in Little Jason Lagoon (Co1305), which confirms the mixed composition of terrigenous OM (Berg et al. 2020) and is within the range of $\Delta^{14}C$ values found in surface soils (Shi et al. 2020). For the mixing models we, thus, use a $\Delta^{14}C_{terr}$ of -16 ± 138‰.

For the Cumberland Bay sites, the isotope mixing models indicate slightly higher incorporation of OC_{terr} based on fatty acids (3.2–11.9%) than on GDGTs (1.9–3.6%), with exception of site PS81/283, which contains 2.5 ± 0.3 $\%OC_{terr}$ based on FA_{terr} and 13.4 ± 0.8% based on $GDGT_{terr}$ (Fig. 4; Supporting Information Table S2). Analogous to the biomarker ratios, differences are large for Little Jason Lagoon, where estimates for $\%OC_{terr}$ based on GDGTs are 76.1–87.2%, but 8.1–15.1% for fatty acids (Fig. 4a). As outlined above, both biomarker ratios may be biased due to alternative biomarker source contributions, an effect, which seems to be particularly strong in the shallow marginal inlet, but rather negligible for the fjord sediments.

Estimates of petrogenic OM ($\%OC_{petro}$) in Cumberland Bay range from 28.6 ± 2.1% at site PS81/284 to 73.8 ± 2.6% at site PS81/283 (Fig. 3) and are lower at the sites without direct glacier input: 14.0 ± 2.5% on the shelf (site PS81/280) and in the marine inlet (e.g., 4.2–10.1 $\%OC_{petro}$ at site Co1303). Irrespective of the biomarker ratios used, mixing models provide similar $\%OC_{petro}$ for sites in Cumberland Bay and on the shelf (Fig. 4). For Little Jason Lagoon, values show large

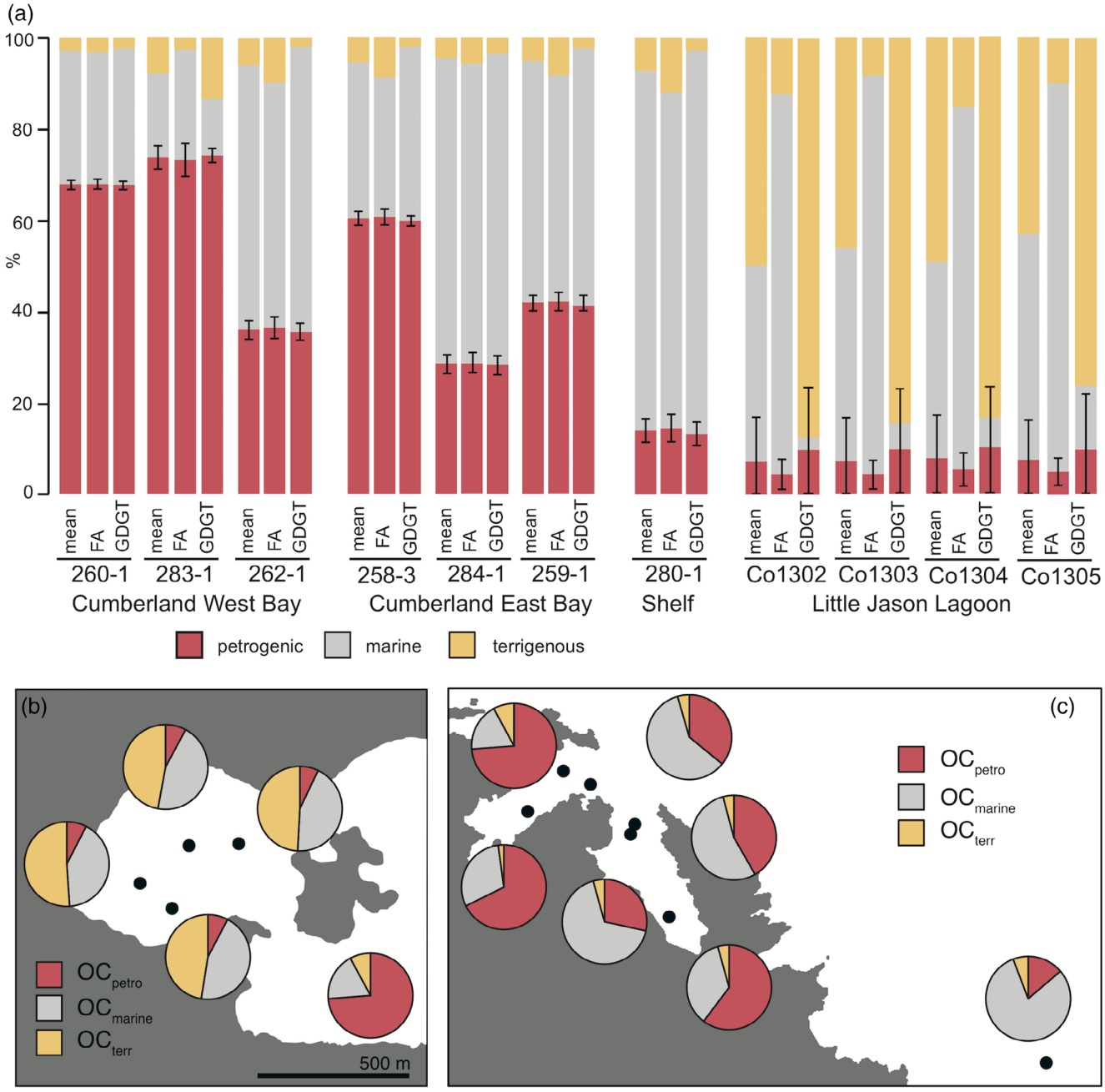

Fig 4. (**a**) Contributions of petrogenic, marine and terrigenous OC in surface sediments in Little Jason Lagoon, Cumberland bays and from the shelf site PS81/280 derived from the mixing model. Results are shown for calculations based on fatty acids (FA) and GDGT ratios. Mean values were calculated as the mean of both models for each site. (**b**) Pie charts showing the mean distribution of petrogenic, marine and terrigenous contributions at each investigated site.

differences and mass balance calculations for some $\Delta^{14}C$ endmember combinations cannot be solved for given $\%OC_{terr}$ based on GDGT ratios. This indicates that the terrigenous contribution may indeed be overestimated by the brGDGT/(brGDGT + crenarchaeol) ratio. Alternatively, the $\Delta^{14}C$ isotopic composition of the terrigenous endmember would have to be less ^{14}C-depleted than assumed. This would imply that only the uppermost peat layers are exported to the fjord, which is not supported by the $C_{26:0}$ fatty acid $\Delta^{14}C$ value of −116‰ (corresponding to 910 ± 105 ^{14}C yr) from core Co1305 that indicates input of pre-aged OC_{terr} into the inlet (Berg et al. 2020).

In the following, we will use the $\%OC_{terr}$ and $\%OC_{petro}$ estimates presented above to calculate the respective MARs and

provide estimates of OC_{terr} and OC_{petro} sequestration in the fjord before and after glacier retreat in recent decades.

OC sequestration in Cumberland Bay

Allochthonous petrogenic and biospheric OC burial in Cumberland Bay fjords

On the basis of the OC source quantification in the fjord sediments, we calculate MARs of OC_{terr} and OC_{petro} for each site to determine OC burial in the Cumberland Bay fjords (*see* Supporting Information for description of MAR calculations). In contrast to the terrigenous proportion of OC deposited in Cumberland Bay, which is neutral with respect to the atmospheric carbon budget, OC_{petro} is a potential source of CO_2 to the atmosphere, if this previously sequestered OC pool is remineralized rather than reburied in the fjord. OC_{petro} accounts for a large proportion of OC in the fjord, and MAR of OC_{petro} (MAR_{petro}) and OC_{petro} burial in the fjord will be discussed in more detail in the following.

OC_{petro} is the dominant OC fraction at sites proximal to the glacier calving fronts in Cumberland Bay (Fig. 4b). % OC_{petro} is lower further towards the ocean-ward end of Cumberland Bay and on the shelf. This pattern suggests that glacial erosion and glacial discharge by the calving glaciers control OC_{petro} input and burial in the fjord. In the adjacent Little Jason Lagoon, OC_{petro} is lower irrespective of the uncertainty in assigning biomarker ratios to OC sources in this specific environment (Fig. 4b).

To identify whether the decrease in OC_{petro} is an effect of dilution by contemporaneous OC (e.g., higher vegetation density in the catchment in the outer fjord, higher phytoplankton productivity due to higher light penetration in the water column) or due to successive settling of detrital matter in the fjord, we compare MAR_{petro} throughout the fjord. MAR_{petro} range from 1.3 to 2.4 g OC m^{-2} yr^{-1} at the glacier distal sites to 6.0 g OC m^{-2} yr^{-1} at site PS81/258 close to the calving front of Nordenskjöld Glacier and 9.1 and 6.7 g OC m^{-2} yr^{-1} at sites PS81/283 and PS81/260, respectively, proximal to Neumayer Glacier (Fig. 5b; Supporting Information Table S4). These MAR values represent minimum estimates since they are based on the sedimentation rate estimated at site PS81/283 (for which downcore data are available; *see* Supporting Infomation), while sedimentation rates for PS81/258 and PS81/260 are likely higher due to their proximity to the glaciers. Nevertheless, the trend of decreasing MAR_{petro} with increasing distance to the glacier is evident in the data set, highlighting effective sequestration of OC_{petro} in the fjord.

Only few studies distinguished OC_{petro} from other OC sources when quantifying OC burial in fjords so far. A study found MAR_{petro} of 30–1113 g OC m^{-2} yr^{-1} for glaciated fjords in Southeast Alaska (Cui et al. 2016*b*). These values are much higher than those found for Cumberland Bay, highlighting the effects of site-specific characteristics on MAR_{petro}: the total amount of OC_{petro} discharged into the fjord is likely a function of the size of the drainage area, subglacial erosion rates, and OC content of eroded bedrock lithologies, while the actual MAR_{petro} is likely also affected by the morphology and hydrology of individual fjords as well as the remineralization rate and potential priming effects. Unfortunately, no data are available that allows calculating the amount of OC_{petro} initially discharged by the glaciers in Cumberland Bay. This lack of data prevents us from estimating the proportion of OC_{petro} that is remineralized vs. the proportion buried in fjord sediments, a prerequisite for the assessment of possible CO_2 feedbacks (as has been shown for rivers, e.g., by Rosenheim et al. 2013).

MAR of OC_{terr} (MAR_{terr}) in Cumberland Bay is 0.5 ± 0.3 g OC m^{-2} yr^{-1} and is relatively uniform throughout the fjord (Fig. 5d; Supporting Information Table S4). MAR_{terr} in Cumberland Bay is low compared to fjord environments in other regions, which range from 10.2 g OC m^{-2} yr^{-1} in Chilean fjords to 70.3 g OC m^{-2} yr^{-1} in SE Alaskan fjords (Cui et al. 2016*b*) or 6.3–29.0 g OC m^{-2} yr^{-1} in Storfjorden, Spitsbergen (Winkelmann and Knies 2005). While MAR_{terr} in Storfjorden is controlled by high %OC in the sediments, MAR_{terr} in Cumberland Bay is controlled by high sedimentation rates, which are c. 10 times higher than in Storfjorden, while %OC contents are c. 5 times lower. This suggests that the sediments supplied to Cumberland Bay are low in OC_{terr} compared to Spitsbergen and likely other regions with higher MAR_{terr} (Smith et al. 2015; Cui et al. 2016*b*). The low contribution of terrigenous OC in the sub-Antarctic fjord is likely a function of the sparse vegetation and soil coverage of the terrestrial catchment (with respect to areal coverage and soil thickness, Supporting Information Fig. S3). Erosion of re-exposed, eroded terrestrial deposits, which are a source of terrigenous OC in the Arctic (e.g., Winkelmann and Knies 2005; Vonk et al. 2019) as well, could locally affect MAR_{terr} in Cumberland Bay. For example, at site PS81/258, which is proximal to the eastern flank of Nordenskjöld Glacier in Cumberland East Bay, slightly higher MAR_{terr} (0.5 g OC m^{-2} yr^{-1}, Fig. 5d) may reflect erosion of previously glacier-buried peat deposits (Gordon 1987). However, on a regional scale, this source of OC_{terr} is likely of minor importance, since the formation and preservation of soils is restricted by the steep topography of the island and re-exposure of older deposits is most likely limited to coastal areas (*see* Supporting Information).

In Little Jason Lagoon, the mean MAR_{terr} of 32.7 ± 1.2 g OC m^{-2} yr^{-1} (Fig. 5c; Supporting Information Table S4) is almost 10 times higher than in the fjord. The higher OC_{terr} accumulation is likely due to the proximity to relatively thick soil and peat deposits (Supporting Information Figs. S1, S2) and the morphology of the Little Jason Lagoon catchment, which has a focusing effect for terrigenous OM input from surficial run-off. Annual OC_{terr} burial in the inlet equals c. 30% of OC_{terr} burial in Cumberland West Bay, indicating that coastal inlets like Little Jason Lagoon sequester high amounts of OC_{terr} and may act as hotspots for OC_{terr} burial on South

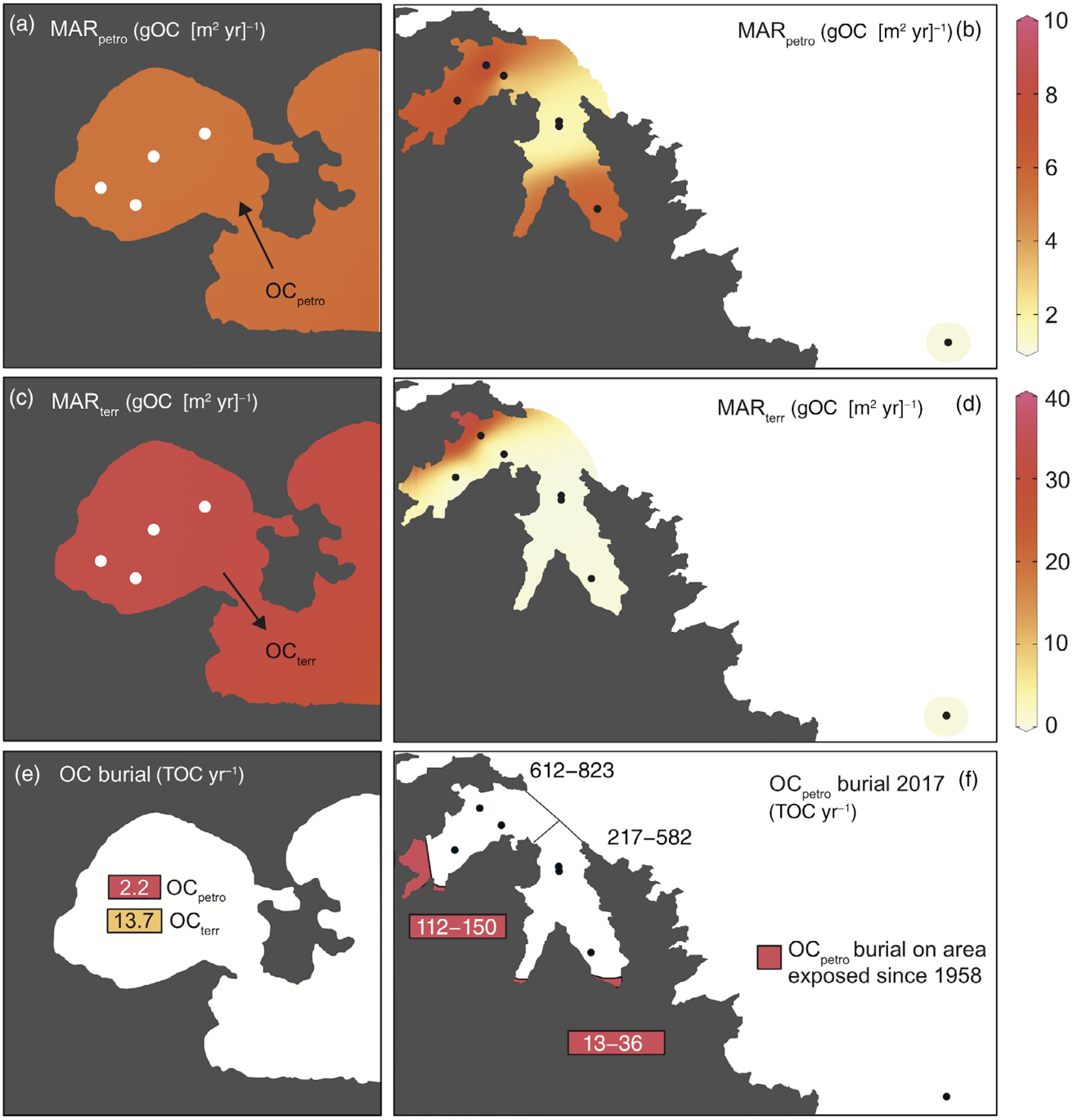

Fig 5. (**a**,**b**) Proportions of petrogenic and terrigenous OC in Cumberland Bay and Little Jason Lagoon, (**c**,**d**) MARs of terrigenous and petrogenic OC in Cumberland Bay and Little Jason Lagoon, (**e**) annual burial of petrogenic and terrigenous OC in Little Jason Lagoon and (**f**) burial of petrogenic OC in Cumberland West Bay and Cumberland East Bay in 2017. Area exposed since 1958 is shaded in pink.

Georgia (Fig. 5e,f). High MAR_{terr} at site PS81/283 (Fig. 5d), which is closest to Little Jason Lagoon, suggests that some proportion of OC_{terr} likely escapes deposition in the inlet and is exported into the fjord.

As discussed for site PS81/258, glacial erosion is a possible process that releases OC_{terr} into the fjords. However, the relatively uniform distribution of OC_{terr} in Cumberland Bay (Fig. 4c) indicates that site-specific effects cause higher OC_{terr} input locally. To what extent the glaciers act as focused input pathways for OC_{terr} in South Georgia, such as rivers discharging OC_{terr} from an un-glaciated hinterland (e.g., as observed in Norwegian fjords, Faust and

Knies 2019), could be elucidated by studying sites closer to the present-day calving fronts of Cumberland Bay glaciers, which could not be accessed during cruise PS81. MAR_{terr} of 0.6 g OC m^{-2} yr^{-1} at site PS81/280 outside Cumberland Bay indicates that OC_{terr} is also exported to the shelf (Fig. 5c).

Changes in allochthonous OC burial due to recent glacier retreat and potential future implications

In Cumberland Bay, retreat of tidewater glaciers has been documented by aerial photographs and satellite imagery over a period of more than 60 yr (Gordon et al. 2008; Cook et al. 2010; https://sggis.gov.gs). Between 2003 and 2016 area loss at marine and lake-terminating glacier fronts corresponded to 4% of total glacier area (Farias-Barahona et al. 2020). As a consequence, the fjord area of Cumberland West Bay increased by 22.4% relative to 1958 (Fig. 1), which is mostly due to the retreat of the Neumayer Glacier calving front. In Cumberland East Bay, 6.5% of the total fjord area has been exposed from glacier coverage since 1958 increasing the area for sediment accumulation in the fjord. The glaciers are grounded and therefore no sediment deposition occurred under ice prior to glacier retreat. Grounding is reflected in steep surface topographic profiles, heavily crevassed ice tongues and warm water temperatures, which do not support ice shelves.

Although only Neumayer Glacier has shown substantial retreat in recent decades, the increase in thinning and retreat rates of all marine terminating glaciers on the north-eastern side of the island likely is a response to warming climate (Thomas et al. 2018), which affects glaciers in South Georgia in multiple ways. An increase in air temperature has been shown to result in an elevation shift a rise of the glacier equilibrium line, leading to retreat of cirque glaciers on the island (White et al. 2018). The rise in temperature may also cause increasing precipitation and accumulation of snow in the feeding areas of the larger outlet glaciers in higher altitude (Gordon et al. 2008). Finally, marine terminating fjord-calving glaciers may suffer from frontal and basal melt due to the intrusion of warmer deep water on the shelf and into the fjords, which has been detected to incur into Cumberland Bay (Geprägs et al. 2016).

Based on the fjord area and MAR_{petro} for the six coring sites we estimate the total amount of OC_{petro} buried in Cumberland West Bay and Cumberland East Bay per year for 2017 and 1958 (Fig. 5f) allowing us to calculate the additional OC_{petro} burial in the recently exposed fjord areas. Extrapolating MAR_{petro} of the glacier-distal sites to the whole fjord likely underestimates OC_{petro} burial rates considerably for the fjords, since MAR_{petro} are highest off the glacier fronts. We therefore use a range for OC_{petro} burial derived from MAR_{petro} of sites PS81/260 and PS81/258 for glacier-proximal fjord sites (no samples are available from sites closer to the glacier calving fronts), sites PS81/283 and PS81/259 for the glacier distal sites, and site Co1305 for Little Jason Lagoon (*see* Supporting Information). OC_{petro} burial in Cumberland West Bay amounts to 612.5–822.9 t yr^{-1} for the glacier extent observed in 2017 (Fig. 5f). This OC_{petro} burial corresponds to a 112.0–150.5 t yr^{-1} increase relative to the 1958 glacier extent. Burial rates are lower for Cumberland East Bay, where they ranged from 217.1–582.3 t yr^{-1} in 2017. The corresponding increase in OC_{petro} burial relative to 1958 is 13.7–35.7 t yr^{-1}. The lower values most likely reflect the lower retreat rate of Nordenskjöld Glacier that is associated with lower burial of OC_{petro} into Cumberland East Bay due to less area gain in the fjord. On an island-wide scale, area loss of marine and lake-terminating glaciers at their respective glacier fronts was 6.58 ± 0.33 km^2 yr^{-1} for the observation period from 2003 to 2016 alone (Farias-Barahona et al. 2020). Based on the OC_{petro} burial rates determined for Cumberland Bay, the newly exposed area between 2003 and 2016 has the potential to have sequestered 181.8–813.2 t OC_{petro} yr^{-1}, which accounts for 0.01–0.05‰ of annual OC burial in fjords globally (Smith et al. 2015).

To quantify possible feedbacks on carbon cycling by remineralization of OC_{petro}, the burial efficiency of OC_{petro} (defined as the amount of OC_{petro} buried in the fjord sediments relative to the amount initially released/mobilized by the glaciers) needs to be assessed for the fjords in South Georgia. Burial efficiency of OC_{petro} is likely less than 100% in Cumberland Bay, with some proportion being remineralized during transport in the fjords as particulate matter (although remineralization prior to entering the fjord probably is negligible and low water depth fosters rapid burial). The proportion being remineralized cannot be directly estimated from our data set, which lacks meltwater discharge measurements (including particulate matter content). Previous studies report that the burial efficiency of refractory OC_{petro} is c. 70–85% during nearshore lateral transport (Wei et al. 2021) and in settings with high sedimentation rates (Galy et al. 2007). If we use these estimates, we can calculate the amount of OC_{petro} initially released/supplied by the glaciers and the amount that has been remineralized prior to burial. At 70% burial efficiency, 77.9–348.5 t OC_{petro} yr^{-1} would have been remineralized (based on MAR_{petro} calculated for the newly exposed fjord areas). At 85% burial efficiency, approximately 32.1–143.5 t OC_{petro} yr^{-1}would have been remineralized into the atmosphere. We acknowledge that these are just rough estimates, and local burial efficiencies need to be calculated/determined in order to provide accurate data.

We assume the accelerating glacier loss on South Georgia that is presently observed has increased sediment supply to Cumberland Bay due to increased sub-glacial erosion and increased meltwater discharge, as observed elsewhere (Syvitski and Andrews 1994; Overeem et al. 2017). For Cumberland Bay, this will likely result in a future increase in MAR of OC_{petro}, as the sediment discharged by the glaciers is mostly composed of eroded bedrock. Whether such an increase in OC_{petro} input can be compensated for by increased burial, due

to availability of new sediment accommodation space, or will result in a net decrease in OC_{petro} burial efficiency and potentially positive carbon feedback needs to be further investigated.

Successive retreat of the glaciers in Cumberland Bay and elsewhere in South Georgia could also result in re-exposure of older soil and peat deposits, which are a potential additional source of OC, analogous to the Arctic, where OC from formerly frozen permafrost is exported to the ocean (e.g., Vonk et al. 2019; Kusch et al. 2021*a*). In South Georgia, little is known about the existence and spatial distribution of such older terrestrial deposits underneath the glacier ice. While buried Holocene peat and soil deposits were found frequently in terrestrial moraines (e.g., Clapperton et al. 1989; Bentley et al. 2007), Geprägs et al. (2016) suggested peat deposits eroded by glacier-fluvial activity during deglaciation as a likely matrix for methanogenesis in deeper (not yet sampled) sediments in Cumberland Bay. Since these layers are suitable to sustain methanogenesis resulting in methane seeps in the fjord, some proportion of the buried biodegradable OC may yet escape into the ocean/atmosphere (Römer et al. 2014). Based on our results, we show that OC_{terr} is a minor contributor to the fjord sediments at present. A ^{14}C study on land plant derived fatty acids indicates that the terrigenous reservoir in Cumberland West Bay was characterized by centennial to millennial OC storage throughout the Holocene, indicating that the abundance of "old" (pre-Holocene) terrigenous OC is relatively minor (Berg et al. 2020). Hence, re-exposed old OC_{terr} is likely not a prominent source of OC during on-going glacier retreat. Instead, newly exposed land surfaces on centennial time scales may serve as additional areas for soil formation and vegetation that act as CO_2 sinks (e.g., Yoshitake et al. 2011).

While an increase of OC_{terr} and OC_{petro} supply may also increase nutrient supply to the Southern Ocean and affect marine productivity (Borrione and Schlitzer 2013; Barnes et al. 2020), our calculation illustrates that the capacity of OC_{petro} sequestration increases when additional areas in the fjord are liberated by the retreating glacier ice. In this respect, South Georgia may act as an analogue of what might have occurred in the (presently) more temperate fjords at the end of the Last Glacial Maximum as glaciers retreated. Whether the atmospheric feedback caused by remineralization during OC export or heterotrophic respiration and methanogenesis in sediments can be offset by OC burial and soil formation/standing biomass on ground newly exposed be retreating glaciers in this sub-Antarctic environment should be investigated in more detail in future studies.

References

Barnes, D. K. A., and others. 2020. Blue carbon gains from glacial retreat along Antarctic fjords: What should we expect? Global Change Biol. **26**: 2750–2755.

Bentley, M. J., D. J. A. Evans, C. J. Fogwill, J. D. Hansom, D. E. Sugden, and P. W. Kubik. 2007. Glacial geomorphology and chronology of deglaciation, South Georgia, sub-Antarctic. Quat. Sci. Rev. **26**: 644–677.

Berg, S., and others. 2019. Holocene glacier fluctuations and environmental changes in sub-Antarctic South Georgia. Quatern. Res. **91**: 132–148.

Berg, S., S. Jivcov, S. Kusch, G. Kuhn, L. Wacker, and J. Rethemeyer. 2020. Compound-specific radiocarbon analysis of (sub-)Antarctic coastal marine sediments—potential and challenges for chronologies. Paleoceanogr. Paleoclimatol. **35**: e2020PA003890. doi:10.1029/2020PA003890

Bianchi, T. S., and others. 2020. Fjords as Aquatic Critical Zones (ACZs). Earth Sci. Rev. **203**: 103145.

Bohrmann, G. [ed.]. 2013. The expedition of the research vessel "Polarstern" to the Antarctic in 2013 (ANT-XXIX/4). Rep. Polar Mar. Res. **668**: 117–135.

Borrione, I., and R. Schlitzer. 2013. Distribution and recurrence of phytoplankton blooms around South Georgia, Southern Ocean. Biogeosciences **10**: 217–231.

Chen, X., X. Liu, Y. Wei, and Y. Huang. 2019. Production of long-chain n-alkyl lipids by heterotrophic microbes: New evidence from Antarctic lakes. Org. Geochem. **138**: 103909. doi:10.1016/j.orggeochem.2019.103909

Clapperton, C. M., D. E. Sugden, J. Birnie, and M. J. Wilson. 1989. Late-glacial and Holocene glacier fluctuations and environmental change on South Georgia, Southern Ocean. Quatern. Res. **31**: 210–228.

Cook, A. J., S. Poncet, A. P. R. Cooper, D. J. Herbert, and D. Christie. 2010. Glacier retreat on South Georgia and implications for the spread of rats. Antarct. Sci. **22**: 255–263.

Cui, X., T. S. Bianchi, J. M. Jaeger, and R. W. Smith. 2016*a*. Biospheric and petrogenic organic carbon flux along Southeast Alaska. Earth Planet. Sci. Lett. **452**: 238–246.

Cui, X., T. S. Bianchi, C. Savage, and R. W. Smith. 2016*b*. Organic carbon burial in fjords: Terrestrial versus marine inputs. Earth Planet. Sci. Lett. **451**: 41–50.

Cui, X., T. S. Bianchi, and C. Savage. 2017. Erosion of modern terrestrial organic matter as a major component of sediments in fjords. Geophys. Res. Lett. **44**: 1457–1465.

Diefendorf, A. F., and J. Freimuth. 2017. Extracting the most from terrestrial plant-derived *n*-alkyl lipids and their carbon isotopes from the sedimentary record: A review. Org. Geochem. **103**: 1–21.

Eglinton, G., and R. J. Hamilton. 1967. Leaf epicuticular waxes. Science **156**: 1322–1335.

Farias-Barahona, D., and others. 2020. Detailed quantification of glacier elevation and mass changes in South Georgia. Environ. Res. Lett. **15**: 034036.

Faust, J. C., and J. Knies. 2019. Organic matter sources in North Atlantic fjord sediments. Geochem. Geophys. Geosyst. **20**: 2872–2885.

Galy, V., C. France-Lanord, O. Beyssac, P. Faure, H. Kudrass, and F. Palhol. 2007. Efficient organic carbon burial in the Bengal fan sustained by the Himalayan erosional system. Nature **450**: 407–411.

Galy, V., B. Peucker-Ehrenbrink, and T. Eglinton. 2015. Global carbon export from the terrestrial biosphere controlled by erosion. Nature **521**: 204–207.

Geprägs, P., M. E. Torres, S. Mau, S. Kasten, M. Römer, and G. Bohrmann. 2016. Carbon cycling fed by methane seepage at the shallow Cumberland Bay, South Georgia, sub-Antarctic. Geochem. Geophys. Geosyst. **17**: 1401–1418. doi:10.1002/2016GC6276

Gordon, J. E. 1987. Radiocarbon dates from Nordenskjold Glacier, South Georgia, and their implications for late Holocene glacier chronology. Br. Antarct. Surv. Bull. **76**: 1–5.

Gordon, J. E., V. M. Haynes, and A. Hubbard. 2008. Recent glacier changes and climate trends on South Georgia. Global Planet. Change **60**: 72–84.

Graham, A. G. C., and others. 2017. Major advance of South Georgia glaciers during the Antarctic Cold Reversal following extensive sub-Antarctic glaciation. Nat. Commun. **8**: 14798. doi:10.1038/ncomms14798

Hodgson, D. A., A. G. C. Graham, H. J. Giffiths, S. J. Roberts, C. Ó. Cofaigh, M. J. Bentley, and D. J. A. Evans. 2014. Glacial history of sub-Antarctic South Georgia based on the submarine geomorphology of its fjords. Quat. Sci. Rev. **89**: 129–147.

Hopmans, E. C., S. Schouten, and J. S. Sinninghe Damsté. 2016. The effect of improved chromatography on GDGT-based palaeoproxies. Org. Geochem. **93**: 1–6.

Hopmans, E. C., J. W. H. Weijers, E. Schefuß, L. Herfort, J. S. Sinninghe Damsté, and S. Schouten. 2004. A novel proxy for terrestrial organic matter in sediments based on branched and isoprenoid tetraether lipids. Earth Planet. Sci. Lett. **224**: 107–116.

Huguet, C., E. C. Hopmans, W. Febo-Ayala, D. H. Thompson, J. S. Sinninghe Damsté, and S. Schouten. 2006. An improved method to determine the absolute abundance of glycerol dibiphytanyl glycerol tetraether lipids. Org. Geochem. **37**: 1036–1041.

Kim, J.-H., F. Peterse, V. Willmott, D. Klitgaard Kristensen, M. Baas, S. Schouten, and J. S. Sinninghe Damsté. 2011. Large ancient organic matter contributions to Arctic marine sediments (Svalbard). Limnol. Oceanogr. **56**: 1463–1474.

Kusch, S., M. Winterfeld, G. Mollenhauer, S. T. Höfle, L. Schirrmeister, G. Schwamborn, and J. Rethemeyer. 2019. Glycerol dialkyl glycerol tetraethers (GDGTs) in high latitude Siberian permafrost: Diversity, environmental controls, and implications for proxy applications. Org. Geochem. **136**: 103888.

Kusch, S., J. Rethemeyer, D. Ransby, and G. Mollenhauer. 2021*a*. Permafrost organic carbon turnover and export into a high-Arctic fjord: A case study from Svalbard using compound-specific ^{14}C analysis. J. Geophys. Res. Biogeosci. **126**: e2020JG006008. doi:10.1029/2020JG006008

Kusch, S., G. Mollenhauer, C. Willmes, J. Hefter, T. Eglinton, and V. Galy. 2021*b*. Controls on the age of plant waxes in marine sediments—A global synthesis. Org. Geochem. **157**: 104259.

Li, G., L. Li, R. Tarozo, W. M. Longo, K. J. Wang, H. Dong, and Y. Huang. 2018. Microbial production of long-chain *n*-alkanes: Implication for interpreting sedimentary leaf wax signals. Org. Geochem. **115**: 24–31.

McDonald, D. I. M. 1982. Palaeontology and ichnology of the Cumberland Bay formation, South Georgia. Br. Antarct. Surv. Bull. **57**: 1–14.

Orsi, A. H., T. Whitworth, and W. D. Nowlin. 1995. On the meridional extent and fronts of the Antarctic Circumpolar Current. Deep Sea Res. Part I **42**: 641–673.

Overeem, I., B. D. Hudson, J. P. M. Syvitski, A. B. Mikkelsen, M. R. van der Broeke, B. P. Y. Noël, and M. Morlighem. 2017. Substantial export of suspended sediment to the global oceans from glacial erosion in Greenland. Nat. Geosci. **10**: 859–863.

Rethemeyer, J., and others. 2019. Current sample preparation and analytical capabilities of the radiocarbon laboratory at CologneAMS. Radiocarbon **61**: 1449–1460.

Römer, M., and others. 2014. First evidence of widespread active methane seepage in the Southern Ocean, off the sub-Antarctic Island South Georgia. Earth Planet Sci. Lett. **403**: 166–177.

Rosenheim, B. E., K. M. Roe, B. J. Roberts, A. S. Kolker, M. A. Allison, and K. H. Johannesson. 2013. River discharge influence on particulate organic carbon age structure in the Mississippi/Atchafalaya River system. Global Biogeochem. Cycl. **27**: 154–166.

Schouten, S., W. Breteler, P. Blokker, N. Schogt, W. Rijpstra, K. Grice, M. Baas, and J. Damsté. 1998. Biosynthetic effects on the stable carbon isotopic compositions of algal lipids: Implications for deciphering the carbon isotopic biomarker record. Geochim. Cosmochim. Acta **62**: 1397–1406.

Schouten, S., E. C. Hopmans, and J. S. Sinninghe Damsté. 2013. The organic geochemistry of glycerol dialkyl glycerol tetraether lipids: A review. Org. Geochem. **54**: 19–61.

Shi, Z., and others. 2020. The age distribution of global soil carbon inferred from radiocarbon measurements. Nat. Geosci. **13**: 555–559.

Sinninghe Damsté, J. S. 2016. Spatial heterogeneity of sources of branched tetraethers in shelf systems: The geochemistry of tetraethers in the Berau River delta (Kalimantan, Indonesia). Geochim. Cosmochim. Acta **186**: 13–31.

Sinninghe Damsté, J. S., W. I. C. Rijpstra, E. C. Hopmans, M. Y. Jung, J. G. Kim, S. K. Rhee, M. Stieglmeier, and C. Schleper. 2012. Intact polar and core glycerol dibiphytanyl glycerol tetraether lipids of group I.1a and I.1b

Thaumarchaeota in soil. Appl. Environ. Microbiol. **78**: 6866–6874.

Smeaton, C., W. E. N. Austin, A. L. Davies, A. Baltzer, R. E. Abell, and J. A. Howe. 2016. Substantial stores of sedimentary carbon held in mid-latitude fjords. Biogeosciences **13**: 5771–5787.

Smith, R., T. S. Bianchi, M. Allison, C. Savage, and V. Galy. 2015. High rates of organic carbon burial in fjord sediments globally. Nat. Geosci. **8**: 450–453.

Stuiver, M., and H. Polach. 1977. Reporting of ^{14}C data. Radiocarbon **19**: 355–363.

Syvitski, J. P. M., and J. T. Andrews. 1994. Climate change: Numerical modelling of sedimentation and coastal processes, eastern Canadian Arctic. Arc. Alp. Res. **26**: 199–212.

Thomas, Z., and others. 2018. A new daily observational record from Grytviken, South Georgia: Exploring twentieth-century extremes in the South Atlantic. J. Climate **31**: 1743–1755.

Van der Bilt, W. G. M., J. Bakke, J. P. Werner, O. Paasche, G. Rosqvist, and S. Solheim Vatle. 2017. Late Holocene glacier reconstructions reveals retreat behind present limits and two-stage Little Ice Age on Subantarctic South Georgia. J. Quat. Sci. **32**: 888–901. doi:10.1002/jqs.2937

Van der Putten, N., and C. Verbruggen. 2005. The onset of deglaciation of Cumberland Bay and Stromness Bay, South Georgia. Antarct. Sci. **17**: 29–32.

Volkman, J. K., R. B. Johns, F. T. Gillan, G. J. Perry, and H. J. Bavor Jr. 1980. Microbial lipids of an intertidal sediment—I. Fatty acids and hydrocarbons. Geochim. Cosmochim. Acta **44**: 1133–1143.

Volkman, J. K., S. M. Barrett, S. I. Blackburn, M. P. Mansour, E. L. Sikes, and F. Gelin. 1998. Microalgal biomarkers: A review of recent research developments. Org. Geochem. **29**: 1163–1179.

Vonk, J. E., and others. 2019. Temporal deconvolution of vascular plant-derived fatty acids exported from terrestrial watersheds. Geochim. Cosmochim. Acta Theriol. **244**: 502–521.

Wei, B., G. Mollenhauer, J. Hefter, S. Kusch, H. Groheer, E. Schefuß, and G. Jia. 2021. The nature, timescale, and efficiency of riverine export of terrestrial organic carbon in the (sub)tropics: Insights at the molecular level from the Pearl River and adjacent sea. Earth. Planet. Sci. Lett. **565**:116934, doi.org/10.1016/j.epsl.2021.116934.

White, D. A., O. Bennike, M. Melles, and S. Berg. 2018. Was South Georgia covered by an ice cap during the Last Glacial Maximum? In M. J. Siegert, S. S. R. Jamieson, and D. A. White [eds.], Exploration of subsurface Antarctica: Uncovering past changes and modern processes. Geological Society, Special Publications 461. doi:10.1144/SP461.4

Winkelmann, D., and J. Knies. 2005. Recent distribution and accumulation of organic carbon on the continental margin west off Spitsbergen. Geochem. Geophys. Geosyst. **6**: Q09012. doi:10.1029/2005GC000916

Yoshitake, S., M. Uchida, T. Ohtsuka, H. Kanda, H. Koizumi, and T. Nakatsubo. 2011. Vegetation development and carbon storage on a glacier foreland in the High Arctic, Ny-Ålesund, Svalbard. Polar Sci. **5**: 391–397.

Acknowledgments

This study was funded by the Deutsche Forschungsgemeinschaft (DFG) in the framework of the priority program "SPP1158 Antarctic Research with comparative investigations in Arctic ice areas," grant BE 4764/3-1. The fieldwork was carried out within the scope of the *RV* Polarstern cruise PS81; we are grateful to the captain and the crew for their support. We also like to thank the Government of South Georgia and the South Sandwich Islands for providing helpful advice and the permission for fieldwork. Data will be made available via PANGAEA geoscientific database. Open access funding enabled and organized by Projekt DEAL.

Conflict of Interest

None declared.

Submitted 02 March 2021
Revised 10 August 2021
Accepted 03 October 2021

Associate editor: Laura Bristow